Insights into the energy transfer mechanism in Ce^{3+}-Yb^{3+} codoped YAG phosphors

D. C. Yu,[1,2] F. T. Rabouw,[2] W. Q. Boon,[2] T. Kieboom,[2] S. Ye,[1] Q. Y. Zhang,[1,*] and A. Meijerink[2,*]

[1]*State Key Laboratory of Luminescent Materials and Devices, and Institute of Optical Communication Materials, South China University of Technology, Guangzhou 510641, P. R. China*

[2]*Debye Institute for Nanomaterials Science, Utrecht University, P.O. Box 80000, 3508 TA Utrecht, The Netherlands*

(Received 16 May 2014; revised manuscript received 2 September 2014; published 20 October 2014)

Two distinct energy transfer (ET) mechanisms have been proposed for the conversion of blue to near-infrared (NIR) photons in YAG:Ce^{3+},Yb^{3+}. The first mechanism involves downconversion by cooperative energy transfer, which would yield two NIR photons for each blue photon excitation. The second mechanism of single-step energy transfer yields only a single NIR photon for each blue photon excitation and has been argued to proceed via a Ce^{4+}-Yb^{2+} charge transfer state (CTS). If the first mechanism were operative in YAG:Ce^{3+},Yb^{3+}, this material would have the potential to greatly increase the response of crystalline Si solar cells to the blue/UV part of the solar spectrum. In this work, however, we demonstrate that blue-to-NIR conversion in YAG:Ce^{3+},Yb^{3+} goes via the single-step mechanism of ET via a Ce^{4+}-Yb^{2+} CTS. The photoluminescence decay dynamics of the Ce^{3+} excited state are inconsistent with Monte Carlo simulations of the cooperative (one-to-two photon) energy transfer, while they are well reproduced by simulations of single-step (one-to-one photon) energy transfer via a charge transfer state. Based on temperature dependent measurements of energy transfer and luminescence quenching we construct a configuration coordinate model for the Ce^{3+}-to-Yb^{3+} energy transfer, which includes the Ce^{4+}-Yb^{2+} charge transfer state.

DOI: 10.1103/PhysRevB.90.165126 PACS number(s): 42.62.Fi, 78.47.da

I. INTRODUCTION

The ability of photovoltaic cells to convert sunlight into electricity makes them prime candidates for effective large-scale capture and conversion of the sustainable solar energy [1,2]. At present, state-of-the-art commercial single-junction crystalline and polycrystalline Si solar cells dominate the photovoltaic market. While efforts are being made to increase the efficiency of Si solar cells [3–6], the theoretical maximum efficiency (the Shockley-Queisser limit) is no higher than ~30% [7]. Energy losses inherent to the conversion of sunlight to electricity in Si solar cells mainly result from the so-called spectral mismatch between solar spectrum and the band gap of crystalline Si ($E_g \sim 1.12$ eV or 1100 nm) [3,4,6], as pictured in Fig. 1: Subband-gap transmission losses result from incident low-energy photons with energy less than E_g ($E < E_g$) being transmitted rather than absorbed. At the same time, supraband-gap thermalization losses arise because an absorbed high-energy photon with energy more than E_g ($E > E_g$) generates a single "hot" electron-hole pair that rapidly thermalizes to the edges of the conduction band and valence band and loses its excess energy ($E_{\text{photon}} - E_g$) [6].

A promising method to reduce the effect of these intrinsic loss mechanisms in solar cells is by modification of the incident solar spectrum prior to absorption [3,4]. In the process called upconversion two or more low energy photons ($E < E_g$) are added to one higher energy photon that can subsequently be absorbed by the solar cell [8], thus reducing subband-gap transmission losses. The reverse process of downconversion (also named quantum cutting or quantum splitting) converts one high energy photon ($E > 2E_g$) into two or more lower energy photons that can both be absorbed by the solar cell [9], thus reducing supraband-gap thermalization losses. Figure 1 shows the potential power gain for a crystalline Si solar cell enabled by up- and downconversion. Without spectral conversion methods, the spectral mismatch alone (not including other loss mechanisms) leads to an intrinsic 51% loss [compare the AM1.5D spectrum (yellow curve) to the maximum fraction of power converted (green area)]. An additional 13% of the solar power (in the infrared region of the spectrum; red area in Fig. 1) can potentially be utilized by Si solar cells via a two-photon upconversion, while a two-photon downconversion could make an additional 10% available [in the blue/ultraviolet (UV) region; blue area in Fig. 1]. Indeed, with an ideal downconverting material the actual efficiency of a crystalline Si solar cell can be improved to about 40%, well beyond the Shockley-Queisser limit [10].

Recently, visible-to-near-infrared (NIR) downconversion has been extensively investigated in RE^{3+}/Yb^{3+} (RE = Tb, Tm, Pr, Er, Nd, and Ho) codoped materials for the potential application of efficiency enhancement for Si solar cells [5,6,11–18]. The energy of a blue/UV photon absorbed by a RE^{3+} donor ion is transferred to two nearby Yb^{3+} acceptor ions, efficiently emitting two NIR photons around 1000 nm just above the E_g of Si. The energy level structure of the $4f^{13}$ configuration in Yb^{3+} is very simple, with only the $^2F_{7/2}$ ground state and the $^2F_{5/2}$ excited state, separated by ~10 000 cm^{-1} [5,6]. This allows Yb^{3+}, via cross relaxation or cooperative energy transfer, to efficiently accept (part of) the excitated state energy of nearby RE^{3+} donor ions and emit it as a usable NIR photon. However, the intra-$4f$ forbidden transitions involved in RE^{3+} donor ions are characterized by small absorption cross sections (typically on the order of 10^{-21} cm^2) and narrow absorption linewidths [19]. Hence, the first step of the downconversion process, the absorption of the blue/UV photon, is quite inefficient. This greatly limits the practical application of such RE^{3+}/Yb^{3+} codoped downconverting materials.

*Authors to whom correspondence should be addressed: qyzhang@scut.edu.cn and a.meijerink@uu.nl

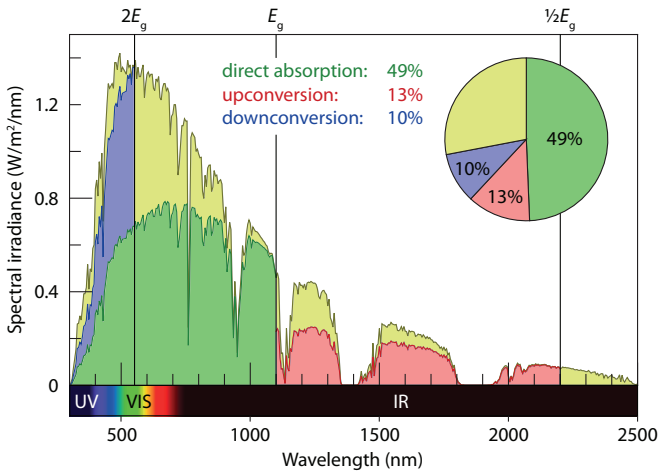

FIG. 1. (Color online) The AM1.5D solar spectrum (yellow curve) illustrating the fraction that can directly be converted by crystalline Si solar cells (green area), and the additional solar power that can be utilized through 1-to-2 downconversion (blue area) and 2-to-1 upconversion (red area).

As an improved solution, alleged broadband NIR downconversion has been reported recently in a variety of Ce^{3+}/Yb^{3+} codoped materials like YAG:Ce^{3+},Yb^{3+} [19–22]. In these materials the Ce^{3+} donor ions, based on allowed $4f \rightarrow 5d$ electric-dipole transitions, have much larger absorption cross sections (typically 10^{-18} cm^2) than $4f \rightarrow 4f$ transitions RE^{3+} donor ions (typically 10^{-21} cm^2). Ideally, an excited Ce^{3+} donor ion would, via cooperative energy transfer, efficiently transfer its energy to two nearby Yb^{3+} acceptor ions leading to the emission of two NIR photons around 1000 nm [19–24]. However, the energy transfer process involved in the Ce^{3+}/Yb^{3+} couple is still under debate [22,25]. The formation of a Ce^{4+}-Yb^{2+} charge transfer state (CTS) has been reported in various materials codoped with the Ce^{3+}/Yb^{3+} couple [26–28]. Ce^{3+}-to-Yb^{3+} energy transfer via such a CTS would result in luminescence downshifting rather than downconversion, i.e., the conversion of one blue/UV photon absorbed by Ce^{3+} to only a single NIR photon re-emitted by Yb^{3+}. As a consequence, the actual Ce^{3+}-to-Yb^{3+} energy transfer mechanism crucially determines whether the Ce^{3+}/Yb^{3+} couple (as an alleged downconverting couple) is potentially useful for increasing solar cell efficiencies.

In this paper we demonstrate that Ce^{3+}-to-Yb^{3+} energy transfer in YAG takes place via a single-step mechanism via a Ce^{4+}-Yb^{2+} CTS. To establish the nature of the energy transfer mechanism YAG:1% Ce^{3+},x% Yb^{3+} ($x = 1, 2, 5, 10,$ and 20) phosphors are studied using (time-resolved) emission and excitation spectroscopy. We systematically vary the Yb^{3+} acceptor concentration, and record photoluminescence decay curves of the emission from Ce^{3+} donor ions. Comparison with models of how the decay dynamics should depend on acceptor concentration, we find that the experimental results are only consistent with the single-step mechanism via a CTS. Moreover, visible-to-NIR emissions and decay curves of Ce^{3+} are measured for YAG:1% Ce^{3+},5% Yb^{3+} in the temperature range between 50 and 290 K. From the observations we construct a configuration coordinate diagram based on the Mott-Seitz model, which explains the temperature activated single-step Ce^{3+}-to-Yb^{3+} energy transfer via a Ce^{4+}-Yb^{2+} CTS, and temperature quenching of the Yb^{3+} emission as the temperature increases above 110 K.

II. EXPERIMENT

Microcrystalline samples of YAG:0.1% Ce^{3+} and YAG:1% Ce^{3+},x% Yb^{3+} ($x = 1, 2, 5, 10,$ and 20) were prepared via solid state techniques based on combustion of lanthanide precursors and reaction of the reactive oxides obtained with alumina at ∼1500 °C. Emission and excitation spectra of YAG:Ce^{3+},Yb^{3+} at room temperature were measured with an Edinburgh Instruments FLS920 spectrofluorometer (with gratings blazed at 300, 500, and 1200 nm) equipped with a red-sensitive Hamamatsu R928 photomultiplier tube (PMT) for the wavelength range of 400–800 nm or a liquid nitrogen-cooled Hamamatsu R5509-72 PMT for the 800–1600 nm region, and a 450 W xenon lamp as the excitation resource. The temperature dependent emission spectra in the 400 to 1100 nm range of YAG:1% Ce^{3+},5% Yb^{3+} were measured with a liquid-nitrogen-cooled charge coupled device (CCD, Princeton Instruments 300i) detector coupled to a 0.3 m Acton Research monochromator. Photoluminescence decay curves of Ce^{3+} emission at 530 nm (Ce^{3+}: $5d \rightarrow 4f$) were recorded on an Edinburgh FLS920 system equipped with a fast Hamamatsu H7422-02 PMT (high sensitivity in the 300–870 nm wavelength range, rise time 0.78 ns) using an Edinburgh Instruments EPL445 picosecond pulsed diode laser (λ_{em} = 441.4 nm, pulse width 80 ps) as the excitation source. Decay curves of the Yb^{3+} emission at 1029 nm (Yb^{3+}: $^2F_{5/2} \rightarrow {}^2F_{7/2}$) were recorded on an Edinburgh FLS920 system combined with a Hamamatsu R5509-42 PMT (higher sensitivity in NIR region compared to the R5509-72 PMT) using an optical parametric oscillator (OPO) system (Opotek HE 355 II) pumped by the third harmonic of a Nd:YAG laser (continuous tunable optical range in 410–2400 nm with a pulse width of 10 ns and a repetition rate of 20 Hz) as the excitation source. To allow for a quantitative comparison of emission intensities, all the optical measurements were performed under identical conditions for each series of tests.

III. MODELING

We model the decay dynamics of the Ce^{3+} excited state and the influence of energy transfer to Yb^{3+} for three different scenarios of the energy transfer mechanism: (1) energy transfer via a CTS, (2) single-step energy transfer via dipole-dipole coupling, and (3) cooperative energy transfer (= quantum cutting) via dipole-dipole coupling. Using Monte Carlo modeling, the distinction between scenarios 2 and 3 has previously been made to establish the occurrence of cooperative energy transfer from Tb^{3+} to Yb^{3+} in YPO_4:Tb^{3+},Yb^{3+} [11], and single-step energy transfer from Pr^{3+} to Yb^{3+} in $LiYF_4$:Pr^{3+},Yb^{3+} [16]. Here we make use of an analytical model for the decay dynamics in scenarios 1 and 2 (charge transfer and single-step dipole-dipole), and Monte Carlo simulations for scenario 3 (cooperative quantum cutting). Both the Monte Carlo procedure and the analytical models take into account that each donor ion (here, Ce^{3+}) has a different "environment"

of nearby acceptor ions (Yb^{3+}). More precisely, although the crystalline host fixes the possible donor-acceptor distances, for each particular donor the actual occupation of cation sites by acceptors is subject to statistics. A particular environment results in a decay rate of the donor ion, depending on the exact number and locations of the nearby acceptor ions.

Energy transfer via a CTS (where one donor ion transfers its energy to one acceptor ion) is basically a tunneling process that depends on wave function overlap. We hence assume that, in analogy with energy transfer via exchange interaction, the energy transfer rate in scenario 1 is exponentially dependent on the donor-acceptor separation [29,30]. The decay rate for a particular environment is then given by

$$\Gamma = \gamma_0 + C \sum_i^{\text{acc.}} \exp(-r_i/d), \tag{1}$$

where γ_0 is the intrinsic decay rate of a donor ion (in the absence of acceptors), and the energy transfer rate is parametrized by a strength C and an interaction range d. The summation runs over all nearby acceptors at distances r_i from the central donor. Alternatively, for the single-step dipole-dipole mechanism (scenario 2) the decay rate of a donor is [16]

$$\Gamma = \gamma_0 + C \sum_i^{\text{acc.}} \frac{1}{r_i^6}, \tag{2}$$

where again C is a prefactor representing the energy transfer strength. Finally, for the cooperative mechanism (scenario 3) that leads to quantum cutting, the decay rate of a donor is given by [11]

$$\Gamma = \gamma_0 + C \sum_i^{\text{acc.}} \sum_{j>i}^{\text{acc.}} \frac{1}{r_i^6 r_j^6}, \tag{3}$$

where again C is the energy transfer strength, and the summation now runs over all acceptor pairs (i, j) at distances (r_i, r_j) from the donor ion.

We have previously shown that, if we neglect donor-to-donor energy migration, in a crystal with overall acceptor concentration x the decay dynamics due to single-step dipole-dipole energy transfer (scenario 2) follow [31]:

$$I(t) = e^{-\gamma_0 t} \prod_i^{\text{shells}} \left(1 - x + x e^{-Ct/r_i^6}\right)^{n_i}, \tag{4}$$

where the summation runs over all "shells" of cation sites surrounding a central donor ion, r_i are the possible donor-acceptor distances in the crystal, and n_i is the number of cation sites at distance r_i. Analogously, for energy transfer via a CT state (scenario 1) the decay dynamics is expected to follow the relation

$$I(t) = e^{-\gamma_0 t} \prod_i^{\text{shells}} \left(1 - x + x e^{-Ct \exp(-r_i/d)}\right)^{n_i}, \tag{5}$$

where it should be noted that this is the same analytical equation that would describe energy transfer via exchange interaction [29]. In the case of the cooperative energy transfer process (scenario 3) there is no analytical expression for the decay dynamics. To get a model that we can fit to experimental data, we perform Monte Carlo simulations. We generate a large number ($N = 10\,000$) of donor environments and, by performing the summations of Eq. (3), express the corresponding donor decay rates in terms of the intrinsic donor decay rate γ_0 and the energy transfer parameter C. The experimental decay curve is simulated by averaging over the environments [32]:

$$I(t) = \frac{1}{N} \sum_{k=1}^{N} \exp[-\Gamma_k(\gamma_0, C)t], \tag{6}$$

where Γ_k is the decay rate of a donor in environment k, which is dependent on γ_0 and C. Note that the influence of the overall acceptor concentration on the decay curve is captured by the distribution of Γ_k values, since the average acceptor concentration is taken into account while generating random environments. The higher the overall acceptor concentration, the higher the probably for a configuration with many nearby acceptors. We can use the model decay curves of Eq. (5) for energy transfer via a CT state, Eq. (4) for single-step energy transfer via dipole-dipole interaction, or Eq. (6) for cooperative energy transfer to fit experimental data and obtain values for γ_0, C.

IV. RESULTS AND DISCUSSION

Figure 2 presents (a) excitation and (b) emission spectra for YAG:1% Ce^{3+},x% Yb^{3+} with x varying from 1 to 20. Under excitation at 455 nm, we observe a broad emission band centered around 530 nm originating from the allowed electronic transition from the $5d^1$ excited state to the $4f$ ground state of Ce^{3+}, as well as the intense NIR emission peaked at 1029 nm characteristic for the intraconfigurational $^2F_{5/2} \rightarrow {}^2F_{7/2}$ transition of Yb^{3+} [19–25]. Figure 2(a) reveals that the excitation spectra of the Ce^{3+} (570 nm) and Yb^{3+} (1029 nm) emission are very similar. The two excitation bands at 340 and 460 nm are due to transitions of the Ce^{3+} ion from the $4f$ ground state to different crystal field components of the $5d$ excited state. We conclude from the excitation

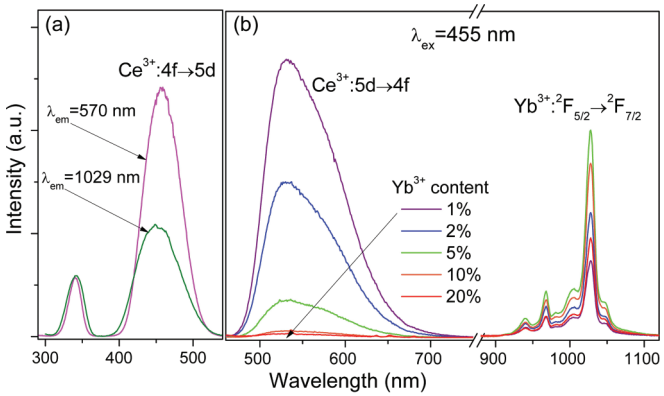

FIG. 2. (Color online) (a) Excitation spectra by monitoring the Ce^{3+}: $5d^1 \rightarrow 4f$ emission at 570 nm and the Yb^{3+}: $^2F_{5/2} \rightarrow {}^2F_{7/2}$ emission at 1029 nm in YAG:Ce^{3+}, Yb^{3+}. (b) Visible-to-NIR emission spectra of YAG:Ce^{3+} codoped with various Yb^{3+} concentrations under excitation of Ce^{3+} at 455 nm.

spectra that the Yb^{3+} emission results from absorption by Ce^{3+} followed by Ce^{3+}-to-Yb^{3+} energy transfer. In Fig. 2(b) we can see that with increasing Yb^{3+} concentration the emission intensity of the Ce^{3+}: $5d \rightarrow 4f$ transition (530 nm) decreases rapidly, until at 20 mol. % Yb^{3+} hardly any Ce^{3+} emission can be observed. The Yb^{3+}: $^2F_{5/2} \rightarrow {}^2F_{7/2}$ emission intensity (1029 nm), on the other hand, rises initially to maximum at 5 mol. % Yb^{3+}, and then drops again as Yb^{3+} content is increased further. The decrease in Ce^{3+} emission intensity and the initial rise of the Yb^{3+} emission intensity result from the improved Ce^{3+}-to-Yb^{3+} energy transfer efficiencies at higher Yb^{3+} concentrations. We ascribe the eventual drop of the Yb^{3+} emission intensity to concentration quenching effects, i.e., energy migration among Yb^{3+} ions until an impurity or defect is reached quenches the luminescence at high Yb^{3+} concentrations [11,12]. These spectra confirm that energy transfer from Ce^{3+} to Yb^{3+} does take place efficiently in YAG host lattice. However, more detailed measurements are required in order to distinguish the energy transfer mechanism: cooperative downconversion from one Ce^{3+} ion to two Yb^{3+} centers, or single-step energy transfer possibly through a Ce^{4+}-Yb^{2+} CTS.

The experimental data points in Fig. 3 show the decay dynamics of the Ce^{3+} $5d^1$ excited state as a function of Yb^{3+} acceptor concentration in YAG host lattice. We can see that the decay becomes faster and more multiexponential with the increase of Yb^{3+} concentration from 1 to 20 mol. %. From these decay curves, without any assumptions or complicated modeling procedures, we can already determine the order of the Ce^{3+}-to-Yb^{3+} energy transfer process. To this end, we calculate for each Yb^{3+} acceptor concentration the average decay rate of the Ce^{3+} $5d^1$ excited state as follows [32]:

$$\langle \Gamma \rangle = \left(\frac{\sum_i I_i t_i}{\sum_i I_i} \right)^{-1}, \tag{7}$$

where t_i and I_i are the delay time and number of photon counts in time channel i, respectively. The corresponding results are plotted in Fig. 4. With the increase of Yb^{3+} concentration from 1 to 20 mol. %, the average decay rate scales linearly (solid black trend line) as expected for a single-step energy transfer mechanism, rather than quadratically (dashed line) for a cooperative energy transfer mechanism. This is a direct indication that Ce^{3+}-to-Yb^{3+} energy transfer in YAG is, in fact, not a second-order cooperative one-to-two photon process of downconversion.

In Fig. 3 we additionally show a comparison of the experimental decay curves to the expected decay dynamics for the three possible scenarios. In Fig. 3(a) we fit the data to a model for energy transfer via a CT state [Eq. (5) above], in Fig. 3(b) to single-step energy transfer via dipole-dipole coupling [Eq. (4) above], and in Fig. 3(c) to cooperative energy transfer [Eq. (6) above]. For each scenario we determined the intrinsic decay rate γ_0 from a fit to the lowest-concentration sample of YAG:1% Ce^{3+},1% Yb^{3+}, and then performed a global fit with fixed γ_0 on all five samples to determine the energy transfer strength C and range d (only for the CT mechanism). The insets show the quality of the fits in terms of the χ^2 parameter. It is clear that the CT scenario [Fig. 3(a)]

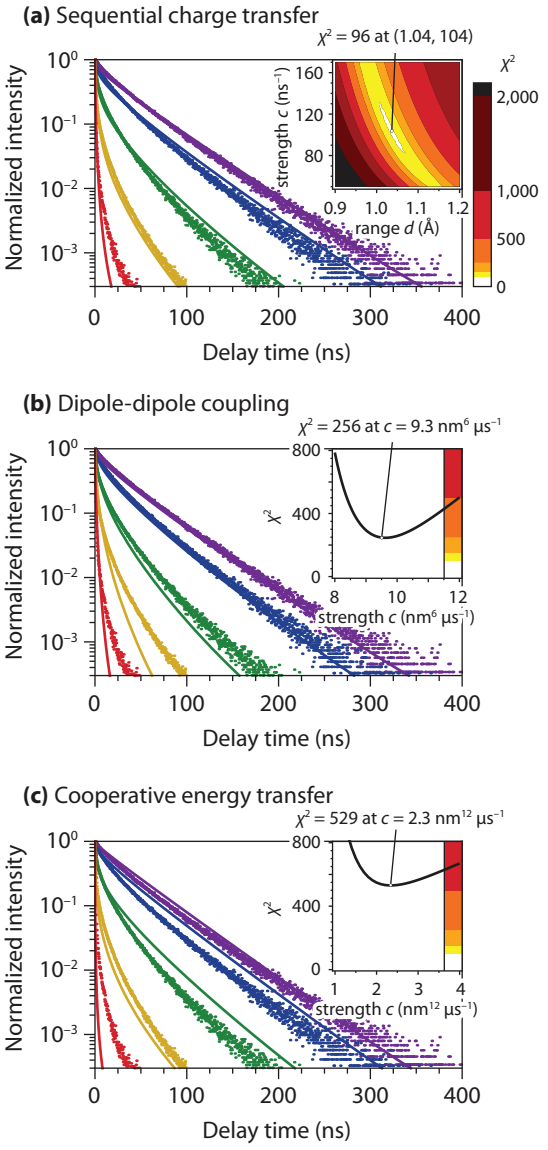

FIG. 3. (Color online) Photoluminescence decay curves of the Ce^{3+}: $5d^1 \rightarrow 4f$ emission at 530 nm in YAG:1% Ce^{3+},x% Yb^{3+} ($x = 1, 2, 5, 10, 20$). The experimental data (dots) are measured upon pulsed laser excitation at 445 nm. Solid lines in (a) show the results of a fit to the model of a single-step energy transfer mechanism via a CTS [Eq. (5)], (b) shows the results of a fit to single-step energy transfer via dipole-dipole coupling [Eq. (4)], while (c) shows the results of a fit to a cooperative energy transfer mechanism [Eq. (6)]. Insets show the quality of the fits.

fits the data best, while fits to the scenarios of single-step dipole-dipole coupling [Fig. 3(b)] and cooperative transfer [Fig. 3(c)] are worse by a factor 2.5 and 5, respectively. These fit results are another strong indication that Ce^{3+}-to-Yb^{3+} energy transfer in YAG is not a cooperative (quantum cutting) process. The fact that the CT model [Fig. 3(a)] fits better than the dipole-dipole model [Fig. 3(b)] is what we would expect based on the energy level structure of the YAG:Ce^{3+},Yb^{3+}; Yb^{3+} does not have an electronic transition resonant with the $5d \rightarrow 4f$ decay of Ce^{3+}. Consequently, energy transfer cannot occur via resonant dipole-dipole coupling (scenario 2).

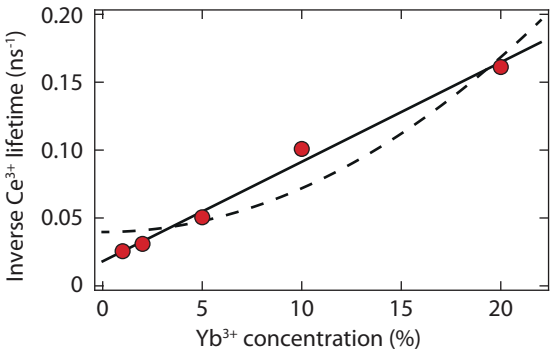

FIG. 4. (Color online) Average decay rate of the Ce^{3+} $5d^1$ excited state as a function of Yb^{3+} concentration in YAG. The solid line shows the linear trend as expected for a single-step energy transfer mechanism, while the dashed line represents a quadratic trend as expected for a cooperative energy transfer mechanism.

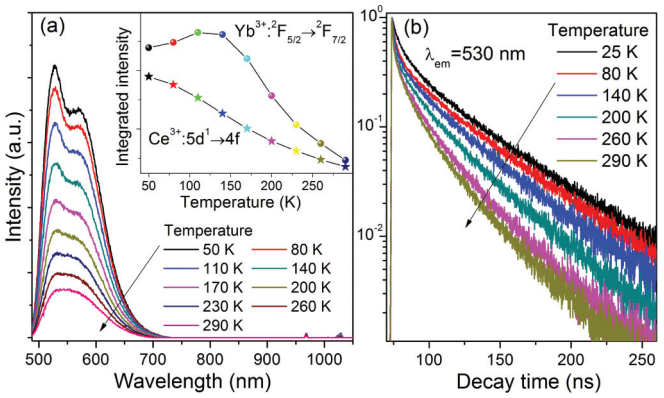

FIG. 5. (Color online) Temperature dependent visible-to-NIR emission spectra (a) and decay curves of Ce^{3+}: $5d^1 \rightarrow 4f$ at 530 nm (b) in YAG:1% Ce^{3+},5% Yb^{3+}. The inset of (a) shows the temperature dependence of the integrated luminescence intensities of the Ce^{3+}: $5d^1 \rightarrow 4f$ and the Yb^{3+}: $^2F_{5/2} \rightarrow {}^2F_{7/2}$ emission.

Instead it must occur via an intermediate CTS (scenario 1). Indeed, thermoluminescence studies of YAG:Ce^{3+},Yb^{3+} have revealed that relaxation from the Ce^{3+} $5d^1$ excited state to a Ce^{4+}-Yb^{2+} CTS is energetically possible in YAG where the Ce^{4+}-Yb^{2+} CTS is approximately 0.8 eV lower in energy [33]. Furthermore, the fitted energy transfer range of $d = 0.10$ nm for the CT process [Fig. 3(a)] is a realistic value for an energy transfer process that requires wave function overlap, which only occurs on atomic scale distances.

It can be observed that the fit of the CT scenario [Fig. 3(a)] is not perfect. The fit underestimates the energy transfer at low acceptor concentration (purple, blue, green), and overestimates it at high acceptor concentrations (yellow, red). These deviations between experiment and model may be due to energy migration among donors. This process increases the probability for the excitation energy to reach acceptors, hence accelerating the decay dynamics. Since the direct donor-to-acceptor transfer is least probable at the lowest acceptor concentrations, the effect of donor-to-donor migration is most pronounced in the low-concentration samples. We note that intrinsic decay rate γ_0 from both models [20.6 μs^{-1} in Fig. 3(a), 20.3 μs^{-1} in Fig. 3(b), and 22.9 μs^{-1} in Fig. 3(c)] is faster than the 12 μs^{-1} observed for a YAG:0.1% Ce^{3+} sample (not shown here), and that is known for YAG:Ce^{3+} at very low Ce^{3+} concentrations [34]. This difference is the result of energy migration and concentration quenching within the Ce^{3+} donor sublattice, which in YAG is already effective at Ce^{3+} concentrations as low as 1 mol. % [34,35].

Previously, Blasse and Grabmaier have shown that by combining one center that tends to become oxidized (e.g., Tb^{3+}, Pr^{3+}, Ce^{3+}) with another center that is easily reduced (e.g., Eu^{3+}, Yb^{3+}), effective quenching can occur through the formation of a RE^{4+}-RE^{2+} CTS [36,37]. Similar to the CTS formation of Tb^{4+}-Yb^{2+} and that of Ce^{4+}-Eu^{2+}, the formation of an intermediate Ce^{4+}-Yb^{2+} CTS involves both photoionization of Ce^{3+} ($Ce^{3+} \rightarrow O^{2-}$) and electron trapping by Yb^{3+} ($O^{2-} \rightarrow Yb^{3+}$) [37]. Indeed, the formation of a Ce^{4+}-Yb^{2+} CTS has been reported in other crystals codoped with Yb^{3+} and Ce^{3+}, including $LiYbF_4$, $YbSiO_5$, and $Yb_xLu_{1-x}PO_4$ [26–28].

To further investigate the energy migration within the Ce^{3+} donor sublattice and the single-step energy transfer dynamics of Ce^{3+}-to-Yb^{3+} via a CTS, the visible-to-NIR emission spectra [Fig. 5(a)] and the decay curves of the Ce^{3+}: $5d^1 \rightarrow 4f$ emission at 530 nm [Fig. 5(b)] were measured for YAG:1% Ce^{3+},5% Yb^{3+} as a function of temperature between 50 and 290 K. In Fig. 5(a) we can see that the photoluminescence intensity of the Ce^{3+} around 550 nm strongly decreases with increasing temperature. This decrease in intensity is consistent with the acceleration of the decay dynamics in Fig. 5(b). Apparently, there is a thermally activated process which quenches emission from the Ce^{3+} $5d$ state. This process can be thermally activated energy transfer to Yb^{3+} via the CTS, energy migration and concentration quenching within the Ce^{3+} sublattice, or a combination of the two. Figure 5(a) further shows that the integrated Yb^{3+}: $^2F_{5/2} \rightarrow {}^2F_{7/2}$ emission increases with temperature below 110 K. This is consistent with thermally activated Ce^{3+}-to-Yb^{3+} energy transfer. However, above 110 K the Yb^{3+} intensity decreases strongly. Clearly there is yet another temperature-dependent process leading to suppression of the Yb^{3+}: $^2F_{5/2} \rightarrow {}^2F_{7/2}$ emission above 110 K.

Figure 6 presents luminescence decay curves of the Yb^{3+}: $^2F_{5/2} \rightarrow {}^2F_{7/2}$ emission recorded at 1029 nm at room temperature, as a function of the Yb^{3+} concentration. The decay time, which is 891 μs for 1 mol. % Yb^{3+} becomes shorter with increasing Yb^{3+} concentration. This is characteristic for concentration quenching by energy migration over the Yb^{3+} sublattice. If we compare the decay curves of 1 and 2 mol. % Yb^{3+} to the one of 5 mol. % Yb^{3+}, we see that for 5 mol. % Yb^{3+} the concentration quenching effect can only account for quenching of the Yb^{3+} emission by at most a factor 2. Clearly another important loss mechanism is involved in the strong drop in Yb^{3+} emission (factor 6) which we found in YAG: 1% Ce^{3+},5% Yb^{3+} above 110 K [Fig. 5(a)]. It should be further noted that we cannot detect any evidence for a rise time in the Yb^{3+} luminescence decay curves for any YAG:Ce^{3+},Yb^{3+} sample under picosecond pulsed laser excitation of the Ce^{3+} $5d$ state. We conclude that the transition

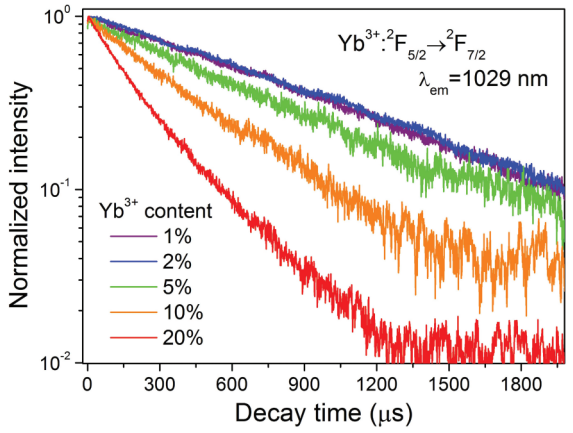

FIG. 6. (Color online) Yb^{3+}-concentration dependent luminescence decay curves of Yb^{3+}: $^2F_{5/2} \rightarrow {}^2F_{7/2}$ at 1029 nm under pulsed laser excitation of Ce^{3+} at 441.4 nm.

from the Ce^{4+}-Yb^{2+} CTS to the Yb^{3+}: $^2F_{5/2}$ state is very fast (nanosecond or faster) [38,39]. Our observation and this conclusion are in contrast with the report of Ueda *et al.* [25] who found a long rise time of 0.2 ms and attributed this to slow relaxation from the Ce^{4+}-Yb^{2+} CTS to the $Yb^{3+2}F_{5/2}$ state. A slow relaxation is unexpected and the luminescence decay curves in Fig. 6 confirm that there is no 0.2 ms relaxation process. Possibly, the rise time observed by Ueda *et al.* is due to an experimental artifact, like saturation of the photomultiplier tube.

Based on the experimental results of Figs. 5 and 6 and the Mott-Seitz model [40], we propose a configuration coordinate model for the Ce^{3+}-to-Yb^{3+} energy transfer in YAG. It is schematically depicted in Fig. 7. After excitation into the Ce^{3+} $5d$ state, a transition is possible to the Ce^{4+}-Yb^{2+} CTS. This transition has an activation barrier ΔE_1, which accounts

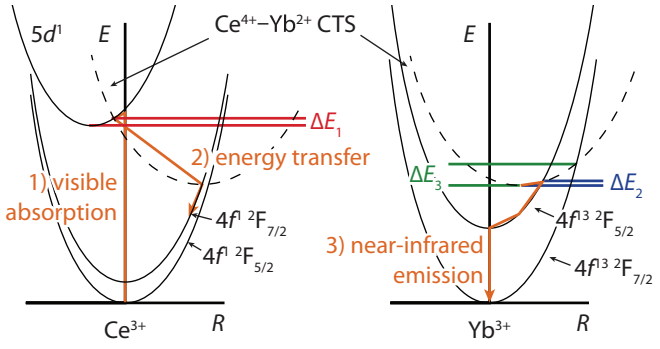

FIG. 7. (Color online) Configuration coordinate model showing the $4f^1$ and $5d$ states of Ce^{3+}, the $4f^{13}$ state of Yb^{3+} (solid parabolas) and the Ce^{4+}-Yb^{2+} CTS (dashed parabolas), illustrating the single-step energy transfer via a Ce^{4+}-Yb^{2+} CTS and the possible pathways of temperature quenching. Entirely nonradiative return to the ground state after excitation of Ce^{3+} to its $5d$ state is possible via the CTS, followed by intersystem crossing over barrier ΔE_3. As it is hard to depict the Ce^{4+}-Yb^{2+} CTS for both ions in a single diagram, the configuration coordinate diagrams of Ce^{3+} and Yb^{3+} are depicted separately.

for the decrease of Ce^{3+} intensity with temperature as well as the increase of Yb^{3+} intensity below 110 K [Fig. 5(a)]. Since Ce^{3+}-to-Yb^{3+} energy transfer is already efficient at 50 K, we conclude that $\Delta E_1 < 5$ meV. From the Ce^{4+}-Yb^{2+} CTS two decay pathways are possible: (1) The transition Ce^{4+}-Yb^{2+} CTS $\rightarrow Ce^{3+}(4f^1)Yb^{3+}(^2F_{5/2})$ leaves Yb^{3+} in the excited $^2F_{5/2}$ state, after which it can emit a NIR photon; and (2) via the transition Ce^{4+}-Yb^{2+} CTS $\rightarrow Ce^{3+}(4f^1)Yb^{3+}(^2F_{7/2})$, on the other hand, Yb^{3+} reaches the $^2F_{7/2}$ ground state nonradiatively. The first pathway has a very low activation barrier $\Delta E_2 \ll 5$ meV, since energy transfer is already efficient at 50 K, the Yb^{3+} emission shows no rise time, and we do not observe any sign of direct emission from a metastable CTS. We estimate the activation barrier for the second (dark) pathway at $\Delta E_3 = 10$ meV, which can account for the strong quenching of the Yb^{3+} emission above 110 K. To summarize, the orange arrow in Fig. 7 depicts the CTS process that leads to visible-to-NIR conversion in YAG:Ce^{3+},Yb^{3+}. At very low temperature <100 K, the energy barrier ΔE_1 is sufficiently high to partially inhibit the energy transfer process, and make direct Ce^{3+} emission efficient [Fig. 5(a)]. At higher temperature >100 K, nonradiative crossover becomes possible over the barrier ΔE_3 to the Yb^{3+} $4f^{13}\,^2F_{7/2}$ ground state, quenching the NIR emission.

Now that we have established that YAG:Ce^{3+},Yb^{3+} does not show quantum cutting, the question rises if quantum cutting by the Ce^{3+}/Yb^{3+} couple is possible in other host materials. Based on the Dorenbos model, which provides relations between the energy levels of the various lanthanides in their 2+ and 3+ oxidation states, we must conclude that the possibility of undesired energy transfer via a Ce^{4+}-Yb^{2+} CTS is general. The relevant energies to consider are those of the Ce^{3+} $5d^1$ excited state relative to the ground state of Yb^{2+}. If the $5d^1$ state of Ce^{3+} is higher in energy than the ground state of Yb^{2+}, charge transfer from the $5d^1$ state of Ce^{3+} to Yb^{3+} is energetically favorable. In the Dorenbos model the energy of both states can be related to the energy of the excited $4f^{13}5d^1$ state of Yb^{2+}. The excited $4f^{13}4d^1$ state of Yb^{2+} is roughly 1.3 eV higher in energy than the excited $4f^05d^1$ state of Ce^{3+} [41]. The energy of the Yb^{2+} ground state ($4f^{14}$) can be estimated from the $4f^{14} \rightarrow 4f^{13}5d^1$ transition energies of Yb^{2+} which are host dependent. Of the more than 300 host compounds listed by Dorenbos, all but one (being EuO) have a higher $4f^{14} \rightarrow 4f^{13}5d^1$ transition energy of Yb^{2+} than YAG and in all compositions the $5d^1$ excited state of Ce^{3+} is situated above the Yb^{2+} ground state [42]. Hence, the estimates from the Dorenbos model lead to the conclusion that Ce^{3+}-to-Yb^{3+} CT from the excited $5d^1$ state of Ce^{3+} is energetically possible in any host.

V. CONCLUSIONS

We have investigated the Ce^{3+}-to-Yb^{3+} energy transfer for the Ce^{3+}/Yb^{3+} couple doped into YAG samples. Comparison of exact simulations of luminescence decay curves of the Ce^{3+} donor for a random distribution of the Yb^{3+} acceptors with the measured decay traces of the Ce^{3+} $5d^1 \rightarrow 4f$ emission reveals that Ce^{3+}-to-Yb^{3+} energy transfer is a

single-step energy transfer via a Ce^{4+}-Yb^{2+} CTS, rather than cooperative downconversion process of 1 $Ce^{3+} \rightarrow$ 2 Yb^{3+}. Based on this it is clear that YAG codoped with a Ce^{3+}/Yb^{3+} couple is not a promising downconversion layer to improve the efficiency of crystalline Si solar cells. We have also investigated the temperature dependence of the energy transfer processes by analyzing photoluminescence spectra and decay curves as a function of temperature. Combination of all experimental results leads to a configuration coordinate model for energy transfer from Ce^{3+} to Yb^{3+} via a Ce^{4+}-Yb^{2+} CTS, which explains the energy transfer as well as the temperature-dependent quenching mechanisms observed.

ACKNOWLEDGMENTS

Financial support from National Science Foundation of China (Grants No. 51125005, No. 21101065, and No. 51472088), Chinese Ministry of Education (Grant No. 20100172110012), and Department of Education of Guangdong Province (Grant No. cxzd1011) are gratefully acknowledged. D. C. Yu would like to thank the China Scholarship Council (CSC, File No. 201206150022) for a scholarship support. This work is part of the research programme of the 'Stichting voor Fundamenteel Onderzoek der Materie (FOM)', which is financially supported by the 'Nederlandse Organisatie voor Wetenschappelijk Onderzoek (NWO)'.

[1] O. Morton, Nature **443**, 19 (2006).
[2] B. van der Zwaan and A. Rabl, Sol. Energy **74**, 19 (2003).
[3] B. S. Richards, Sol. Energy Mater. Sol. Cells **90**, 2329 (2006).
[4] C. Strümpel, M. McCann, G. Beaucarne, V. Arkhipov, A. Slaoui, V. Švrček, C. del Cañizo, and I Tobias, Sol. Energy Mater. Sol. Cells **91**, 238 (2007).
[5] Q. Y. Zhang and X. Y. Huang, Prog. Mater. Sci. **55**, 353 (2010).
[6] B. M. van der Ende, L. Aarts, and A. Meijerink, Phys. Chem. Chem. Phys. **11**, 11081 (2009).
[7] W. Shockley and H. J. Queisser, J. Appl. Phys. **32**, 510 (1961).
[8] T. Trupke, A. Shalav, B. S. Richards, P. Würfel, and M. A. Green, Sol. Energy Mater. Sol. Cells **90**, 3327 (2006).
[9] B. S. Richards, Sol. Energy Mater. Sol. Cells **90**, 1189 (2006).
[10] T. Trupke, M. A. Green, and P. Würfel, J. Appl. Phys. **92**, 1668, (2002).
[11] P. Vergeer, T. J. H. Vlugt, M. H. F. Kox, M. I. Den Hertog, J. P. J. M. van der Eerden, and A. Meijerink, Phys. Rev. B **71**, 014119 (2005).
[12] Q. Y. Zhang, C. H. Yang, and Y. X. Pan, Appl. Phys. Lett. **90**, 021107 (2007).
[13] D. Q. Chen, Y. S. Wang, Y. L. Yu, P. Huang, and F. Y. Weng, Opt. Lett. **33**, 1884 (2008).
[14] J. M. Meijer, L. Aarts, B. M. van der Ende, T. J. H. Vlugt, and A. Meijerink, Phys. Rev. B **81**, 035107 (2010).
[15] J. J. Eilers, D. Biner, J. T. Van Wijngaarden, K. Krämer, H.-U. Güdel, and A. Meijerink, Appl. Phys. Lett. **96**, 151106 (2010).
[16] J. T. van Wijngaarden, S. Scheidelaar, T. J. H. Vlugt, M. F. Reid, and A. Meijerink, Phys. Rev. B **81**, 155112 (2010).
[17] K. M. Deng, T. Gong, L. X. Hu, X. T. Wei, Y. H. Chen, and M. Yin, Opt. Express **19**, 1749 (2011).
[18] D. C. Yu, S. Ye, X. Y. Huang, and Q. Y. Zhang, AIP Adv. **2**, 022124 (2012).
[19] D. Q. Chen, Y. S. Wang, Y. L. Yu, P. Huang, and F. Y. Weng, J. Appl. Phys. **104**, 116105 (2008).
[20] H. Lin, S. M. Zhou, H. Teng, Y. K. Li, W. J. Li, X. R. Hou, and T. T. Jia, J. Appl. Phys. **107**, 043107 (2010).
[21] W. L. Zhou, Y. Li, R. H. Zhang, J. Wang, R. Zou, and H. B. Liang, Opt. Lett. **37**, 4437 (2012).
[22] X. F. Liu, Y. Teng, Y. X. Zhuang, J. H. Xie, Y. B. Qiao, G. P. Dong, D. P. Chen, and J. R. Qiu, Opt. Lett. **34**, 3565 (2009).
[23] J. D. Chen, H. Guo, Z. Q. Li, H. Zhang, and Y. X. Zhuang, Opt. Mater. **32**, 998 (2010).
[24] M. K. Lau and J. H. Hao, J. Nanomater **2013**, 587036 (2013).
[25] J. Ueda and S. Tanabe, J. Appl. Phys. **106**, 043101 (2009).
[26] J. W. M. Verweij, C. Pédrini, D. Bouttet, C. Dujardin, H. Lautesse, and B. Moine, Opt. Mater. **4**, 575 (1995).
[27] D. W. Cooke, R. E. Muenchausen, B. L. Bennett, K. J. McClellan, and A. M. Portis, J. Lumin. **79**, 185 (1998).
[28] J. F. Rivas-Silva, S. Durand-Niconoff, T. M. Schemidt, and M. Berrondo, Int. J. Quantum Chem. **79**, 198 (2000).
[29] D. L. Dexter, J. Chem. Phys. **21**, 836 (1953).
[30] A. H. A. Clayton, G. D. Scholes, K. P. Ghiggino, and M. N. Paddon-Row, J. Phys. Chem. **100**, 10912 (1996).
[31] F. T. Rabouw, S. A. den Hartog, T. Senden, and A. Meijerink, Nat. Commun. **5**, 3610 (2014).
[32] A. F. van Driel, I. S. Nikolaev, P. Vergeer, P. Lodahl, D. Vanmaekelbergh, and W. L. Vos, Phys. Rev. B **75**, 035329 (2007).
[33] F. You, A. J. J. Bos, Q. Shi, S. Huang, and P. Dorenbos, J. Phys.: Condens. Matter. **23**, 215502 (2011).
[34] V. Bachmann, C. Ronda, and A. Meijerink, Chem. Mater. **21**, 2077 (2009).
[35] D. J. Robbins, B. Cockayne, B. Lent, and J. L. Glasper, J. Electrochem. Soc. **126**, 1556 (1979).
[36] G. Blasse and B. C. Grabmaier, *Luminescent Materials* (Springer, Berlin, 1994).
[37] J. L. Yuan, X. Y. Zeng, J. T. Zhao, Z. J. Zhang, H. H. Chen, and X. X. Yang, J. Phys. D: Appl. Phys. **41**, 105406 (2008).
[38] P. Dorenbos, J. Phys.: Condens. Matter. **15**, 2645 (2003).
[39] P. Dorenbos, J. Lumin. **111**, 89 (2005).
[40] G. Blasse, Struct. Bonding **26**, 43 (1976).
[41] P. Dorenbos, J. Lumin. **108**, 301 (2004).
[42] P. Dorenbos, J. Lumin. **104**, 239 (2003).